



Universiteit  
Leiden  
The Netherlands

## **Different microvascular alterations underlie microbleeds and microinfarcts**

Veluw, S.J. van; Scherlek, A.A.; Freeze, W.M.; Telgte, A. ter; Kouwe, A.J. van der; Bacskai, B.J.; ... ; Greenberg, S.M.




### **Citation**

Veluw, S. J. van, Scherlek, A. A., Freeze, W. M., Telgte, A. ter, Kouwe, A. J. van der, Bacskai, B. J., ... Greenberg, S. M. (2019). Different microvascular alterations underlie microbleeds and microinfarcts. *Annals Of Neurology*, 86(2), 279-292.  
doi:10.1002/ana.25512

Version: Publisher's Version  
License: [Creative Commons CC BY 4.0 license](#)  
Downloaded from: <https://hdl.handle.net/1887/3630346>

**Note:** To cite this publication please use the final published version (if applicable).

# Different Microvascular Alterations Underlie Microbleeds and Microinfarcts

Susanne J. van Veluw, PhD <sup>1,2</sup> Ashley A. Scherlek, BM,<sup>1</sup> Whitney M. Freeze, PhD <sup>1,3</sup>  
Annemieke ter Telgte, MSc <sup>1,4</sup> Andre J. van der Kouwe, PhD,<sup>5</sup> Brian J. Bacskai, PhD,<sup>1</sup>  
Matthew P. Frosch, MD, PhD,<sup>1,6</sup> and Steven M. Greenberg, MD, PhD<sup>2</sup>

**Objective:** Cerebral amyloid angiopathy (CAA) is characterized by the accumulation of amyloid  $\beta$  ( $A\beta$ ) in the walls of cortical vessels and the accrual of microbleeds and microinfarcts over time. The relationship between CAA severity and microbleeds and microinfarcts as well as the sequence of events that lead to lesion formation remain poorly understood.

**Methods:** We scanned intact formalin-fixed hemispheres of 12 CAA cases with magnetic resonance imaging (MRI), followed by histopathological examination in predefined areas and serial sectioning in targeted areas with multiple lesions.

**Results:** In total, 1,168 cortical microbleeds and 472 cortical microinfarcts were observed on ex vivo MRI. Increasing CAA severity at the whole-brain or regional level was not associated with the number of microbleeds or microinfarcts. However, locally, the density of  $A\beta$ -positive cortical vessels was lower surrounding a microbleed compared to a simulated control lesion, and higher surrounding microinfarcts. Serial sectioning revealed that for ( $n = 28$ ) microbleeds, both  $A\beta$  (4%) and smooth muscle cells (4%) were almost never present in the vessel wall at the site of bleeding, but  $A\beta$  was frequently observed upstream or downstream (71%), as was extensive fibrin(ogen) buildup (87%). In contrast, for ( $n = 22$ ) microinfarcts, vascular  $A\beta$  was almost always observed at the core of the lesion (91%,  $p < 0.001$ ) as well as upstream or downstream (82%), but few vessels associated with microinfarcts had intact smooth muscle cells (9%).

**Interpretation:** These observations provide a model for how a single neuropathologic process such as CAA may result in hemorrhagic or ischemic brain lesions potentially through 2 different mechanistic pathways.

ANN NEUROL 2019;86:279–292

Cerebral amyloid angiopathy (CAA) is an age-related cerebral small vessel disease that commonly affects the brains of older individuals.<sup>1</sup> Traditionally, CAA has been considered primarily a bleeding disorder based on the observation of multiple microbleeds on brain scans of affected patients and the occurrence of symptomatic lobar intracerebral hemorrhage (ICH).<sup>1,2</sup> More recently, it has become clear that widespread ischemic brain tissue injuries such as white matter hyperintensities and microinfarcts are also prominent features in CAA, most likely contributing

to gradual cognitive decline in these patients.<sup>3–5</sup> Although hemorrhagic lesions (eg, microbleeds) and ischemic lesions (eg, microinfarcts) commonly co-occur in patients with CAA, it remains largely unknown whether they share similar or distinct underlying pathophysiological pathways. Neuropathologically, CAA is characterized by the accumulation of the amyloid  $\beta$  ( $A\beta$ ) peptide in the walls of leptomeningeal and cortical arterioles, which is believed to be the main cause for microbleed and microinfarct formation in affected areas.<sup>6</sup> However, there are few studies that

View this article online at [wileyonlinelibrary.com](http://wileyonlinelibrary.com). DOI: 10.1002/ana.25512

Received Feb 20, 2019, and in revised form May 29, 2019. Accepted for publication May 29, 2019.

Address correspondence to Dr van Veluw, Massachusetts General Hospital, MassGeneral Institute for Neurodegenerative Disease, 114 16th Street, Charlestown, MA 02129. E-mail: [svanveluw@mgh.harvard.edu](mailto:svanveluw@mgh.harvard.edu)

From the <sup>1</sup>MassGeneral Institute for Neurodegenerative Disease, Massachusetts General Hospital and Harvard Medical School, Charlestown, MA;

<sup>2</sup>J. Philip Kistler Stroke Research Center, Department of Neurology, Massachusetts General Hospital and Harvard Medical School, Boston, MA;

<sup>3</sup>Department of Psychiatry and Neuropsychology, Maastricht University, School for Mental Health and Neuroscience, Alzheimer Center Limburg, Maastricht, the Netherlands; <sup>4</sup>Department of Neurology, Donders Institute for Brain, Cognition, and Behavior, Radboud University Medical Center, Nijmegen, the Netherlands; <sup>5</sup>Athinoula A. Martinos Center for Biomedical Imaging, Department of Radiology, Massachusetts General Hospital, Charlestown, MA; and <sup>6</sup>Neuropathology Service, C. S. Kubik Laboratory for Neuropathology, Massachusetts General Hospital and Harvard Medical

School, Boston, MA

have directly assessed the relationship between CAA burden and the occurrence of microbleeds and microinfarcts throughout the brain. Moreover, the exact underlying sequence of events in a single vessel that lead to either a microbleed or a microinfarct in patients with CAA are not fully understood. To fill this gap, we used high-resolution ex vivo magnetic resonance imaging (MRI) combined with histopathology in intact hemispheres to assess the associations between microbleeds and microinfarcts with CAA severity at the whole-brain, regional, and local level. Furthermore, guided by ex vivo MRI, we sampled lesion-rich areas to perform serial sectioning to assess the pathology of microbleeds and microinfarcts at the single-vessel level. Recently, in an exploratory study of single histopathological sections of MRI-targeted microbleeds in areas with severe CAA, we reported absence of A $\beta$  from the wall of the bleeding arterioles at the site of rupture.<sup>7</sup> This observation leads to the question of whether microbleeds in CAA happen (1) because of extensive remodeling of the arteriolar wall (including loss of A $\beta$ ) or (2) in healthy vessels without A $\beta$  that are perhaps more at risk to "take the hit" when the local CAA-affected network (likely stiffened) is under pressure. In this study, we aimed to answer these questions using serial sectioning to uncover the properties of the vessels involved in microbleeds both at the site of rupture as well as upstream and downstream. Moreover, we aimed to extend these observations to microinfarcts, for which the relationship with vascular A $\beta$  is currently unknown.

## Materials and Methods

### Cases

Thirteen intact brains were received through an ongoing brain donation program initiated within the hemorrhagic stroke research group at the Massachusetts General Hospital (MGH) aimed at the evaluation of MRI markers and their underlying histopathology in the context of CAA.<sup>8,9</sup> All cases had received a clinical diagnosis of possible or probable CAA during life.<sup>1</sup> At autopsy, brains were extracted and fixed in 10% formalin for several weeks, after which the hemispheres were separated by a single midsagittal cut. The least affected hemisphere was used for ex vivo MRI scanning and histopathology in the context of this study. The other hemisphere was processed to undergo routine neuropathological examination by a board-certified neuropathologist. One case was excluded from further analysis, because no evidence of CAA was found on routine neuropathological examination. Study approval was received from the MGH institutional review board and informed consent was obtained from the next of kin or another legal representative prior to autopsy.

### Study Design

The experimental design of the study is depicted in Figure 1. First, intact formalin-fixed hemispheres were subjected to high-resolution

ex vivo 3T MRI to detect microbleeds and microinfarcts. Next, the hemispheres were cut in 10mm-thick coronal slabs and standard samples were taken from predefined areas of frontal, temporal, parietal, and occipital cortex. Four adjacent 6 $\mu$ m-thick sections were cut from these samples and stained with hematoxylin & eosin (H&E), Luxol fast blue H&E, A $\beta$ , and glial fibrillary acidic protein (GFAP) to assess regional associations between histopathologically observed microbleeds and microinfarcts and CAA severity. A composite CAA severity score was calculated to assess whole-hemisphere associations between MRI-observed microbleeds and microinfarcts and CAA severity. Finally, 3 additional samples were taken from 3 cases in an area with multiple microbleeds (from temporal cortex from Cases 2 and 10) or microinfarcts (from parieto-occipital cortex from Case 4) that were visible on ex vivo 3T MRI. Samples from Cases 2 and 4 underwent ultra-high-resolution ex vivo 7T MRI scanning to confirm the high number of lesions in those areas. Afterward, all 3 samples underwent complete serial sectioning (6 $\mu$ m-thick sections) to ensure that all lesions were captured. Sections 1, 21, 41, 61, et cetera were stained with H&E to identify microbleeds and microinfarcts, and sections 2, 6, 10, 14, et cetera underwent immunohistochemistry against A $\beta$ . These serial sections were used to assess local and single-vessel associations between microbleeds and microinfarcts and CAA severity. If present, the vessel that could be traced through the core of the lesion was identified as the presumed "culprit" vessel. In addition, for each lesion identified on H&E, spare adjacent sections underwent immunohistochemistry to detect fibrin(ogen) or smooth muscle cells (SMCs).

### Ex Vivo MRI Scanning

The hemisphere to undergo ex vivo 3T MRI was prepared and scanned as described previously.<sup>8</sup> Briefly, it was packed in a plastic bag filled with periodate-lysine-paraformaldehyde and vacuum sealed to remove air bubbles. Next, it was placed in the 32-channel head coil of a whole-body 3T MRI scanner (MAGNETOM Trio; Siemens Healthineers, Erlangen, Germany) and scanned with an overnight protocol, including a T2-weighted turbo-spin echo (TSE) sequence (resolution = 500  $\times$  500  $\times$  500 $\mu$ m<sup>3</sup>) and a gradient-echo fast low angle shot (FLASH) sequence (resolution = 500  $\times$  500  $\times$  500 $\mu$ m<sup>3</sup>).

The 2 smaller samples to undergo ex vivo 7T MRI were prepared and scanned as described previously.<sup>10</sup> Briefly, each sample was placed in a 50ml falcon tube, submerged in Fomblin (Solvay Solexis, Thorofare, NJ), and placed in a custom-built solenoid coil and scanned on a whole-body 7T MRI scanner (MAGNETOM, Siemens Healthineers). The overnight protocol included a T2-weighted TSE sequence (resolution = 100  $\times$  100  $\times$  100 $\mu$ m<sup>3</sup>) and a FLASH sequence (resolution = 75  $\times$  75  $\times$  75 $\mu$ m<sup>3</sup>).

### Ex Vivo MRI Analysis

Scans were processed in FreeSurfer (<https://surfer.nmr.mgh.harvard.edu>) to obtain 3-dimensional (3D) volumes.<sup>11</sup> Microbleeds and microinfarcts were assessed blinded to CAA severity or other histopathologic findings as previously described.<sup>10</sup> Briefly, cortical microbleeds were identified on the gradient-echo and T2-weighted images, appearing as homogeneous round or ovoid foci of low signal

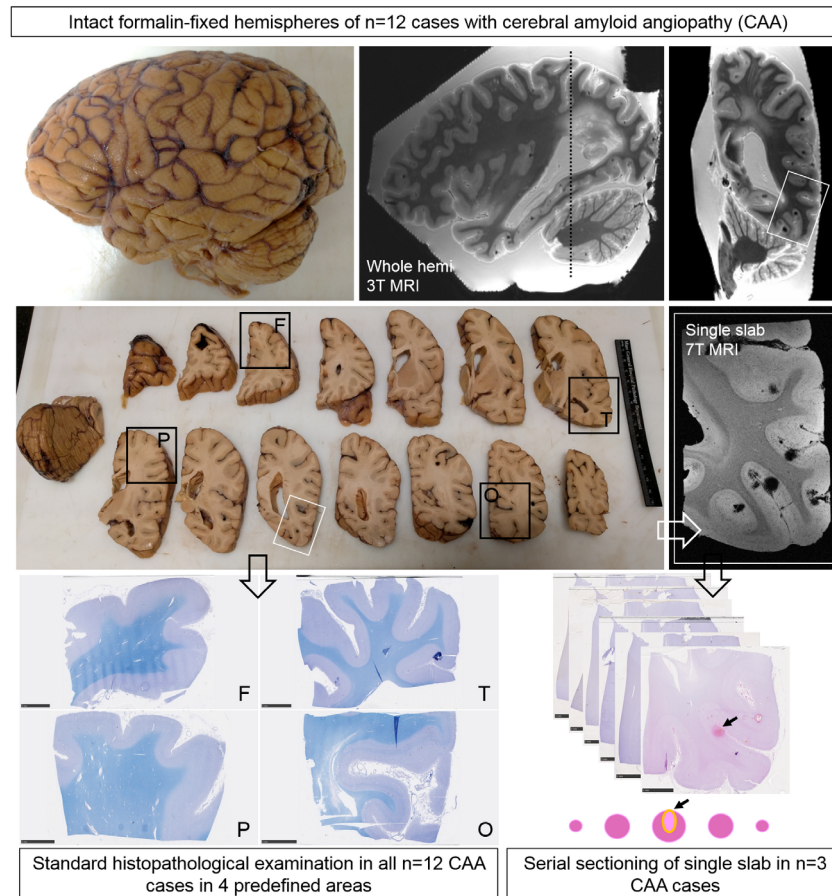


**FIGURE 1: Study design.** Intact formalin-fixed hemispheres of 12 cerebral amyloid angiopathy (CAA) cases were subjected to high-resolution ex vivo 3T magnetic resonance imaging (MRI) to detect microbleeds and microinfarcts. Next, the hemispheres were cut into 10mm-thick coronal slabs and samples were taken from predefined standard areas of frontal (F), temporal (T), parietal (P), and occipital (O) cortex, to fit a standard tissue cassette (black squares). Four adjacent 6 $\mu$ m-thick sections were cut from these samples and stained with hematoxylin & eosin (H&E) or Luxol fast blue H&E (depicted here) and underwent immunohistochemistry to detect amyloid  $\beta$  (A $\beta$ ) and glial fibrillary acidic protein. Finally, 3 additional samples were taken from 3 cases in an area with multiple microbleeds (n = 2, from temporal cortex) or microinfarcts (n = 1, from parieto-occipital cortex) guided by the ex vivo 3T magnetic resonance images (white square). These samples underwent ultra-high-resolution ex vivo 7T MRI scanning to confirm the high number of lesions in those areas. After 7T MRI, the samples were cut in half to fit 2 standard tissue cassettes and underwent complete serial sectioning. Sections 1, 21, 41, 61, et cetera were stained with H&E to identify microbleeds and microinfarcts, and sections 2, 6, 10, 14, et cetera underwent immunohistochemistry against A $\beta$ . If present, the vessel that could be traced through the core of the lesion was identified as the presumed culprit vessel. In addition, for each identified lesion on H&E, sections adjacent to a microbleed or microinfarct underwent immunohistochemistry to detect fibrin(ogen) or smooth muscle cells.

intensity. Cortical microinfarcts were identified on the T2-weighted images, appearing as hyperintense foci within the cortical ribbon. Lesions were annotated using an in-house developed tool, incorporated in MeVisLab (MeVis Medical Solutions, Bremen, Germany). To obtain 3D visualizations of the topographical localization of microbleeds and microinfarcts within each case, annotations were projected on surface renderings of each individual hemisphere.

### Histopathology

Samples taken from predefined standard areas of frontal, temporal, parietal, and occipital cortex and the additional samples that were taken from 3 cases in an area with multiple lesions were processed and embedded in paraffin, after which 6 $\mu$ m-thick sections were cut on a microtome. H&E and Luxol fast blue H&E staining was

performed using standard histology protocols. Bright field immunohistochemistry against A $\beta$  (mouse, clone 6F/3D; Agilent Technologies, Santa Clara, CA; 1:200), GFAP (rabbit, G9269; Sigma, St Louis, MO; 1:1,000), and fibrin(ogen) (rabbit; Dako, Carpinteria, CA; 1:500) was performed as described previously.<sup>8,9</sup> To assess SMCs, sections underwent fluorescent immunohistochemistry to visualize A $\beta$  (rabbit; IBL, Hamburg, Germany; 1:500 and antirabbit Alexa Fluor 350, 1:250, as the secondary), SMCs (mouse, Dako, 1:250 and antimouse Alexa Fluor 488, 1:500, as the secondary), and endothelial cells (DyLight 594-labeled *Lycopersicon esculentum* [Tomato] Lectin; Vector Laboratories, Burlingame, CA; 1:500) within the same vessel. Negative controls were included by omitting the primary antibodies and showed no immunopositivity.

### Histopathology Image Analysis

Digital brightfield microscopic images of the sections were obtained with the NanoZoomer Digital Pathology (NDP)-HT whole slide scanner (C9600-12; Hamamatsu Photonics, Hamamatsu, Japan) equipped with a  $\times 20$  objective. The software NDP.View2 (v2.7.25) was used to assess the obtained digital images. Fluorescent microscopic images were obtained with a Zeiss (Oberkochen, Germany) fluorescent microscope and a  $\times 5$  objective.

Microbleeds and microinfarcts were identified on the H&E-stained sections, using the following criteria. Any area of extravasated (lysed) red blood cells with or without hemosiderin was classified as an acute/recent microbleed. A few hemosiderin deposits at the edges of the lesion were allowed. An area with many focal hemosiderin deposits with or without evidence of hemosiderin was classified as an old/chronic microbleed.<sup>12</sup> Recent/acute microinfarcts were considered areas of tissue pallor with evidence of "red" (ie, hypoxic) neurons. Old/chronic microinfarcts were characterized by tissue loss with cavitation or "puckering" and GFAP positivity around the edges of the lesion.<sup>5</sup> CAA severity was evaluated on the A $\beta$ -stained sections from the predefined standard areas of frontal, temporal, parietal, and occipital cortex using a 4-point scale (absent, 0; scant A $\beta$  deposition, 1; some circumferential A $\beta$ , 2; widespread circumferential A $\beta$ , 3), following proposed consensus criteria.<sup>13</sup> Scores from the 4 areas were added to form a cumulative CAA severity score (Table).

Sholl analysis was performed to assess local CAA burden surrounding microbleeds and microinfarcts, as described previously.<sup>7</sup> From the serial sections from 3 cases, annotated microbleeds and microinfarcts on the H&E-stained sections were included, except when they were located close to another lesion or to an edge of the section. On each section, 2 control areas were selected on H&E (blinded for CAA severity), in a local area without a lesion. Each lesion or control area was localized on the adjacent A $\beta$ -stained section, and images were exported at  $\times 2.5$  magnification. Each lesion was covered with a round or oval-shaped mask in Paint. The same size and shape masks were used for the accompanying control areas to ensure blinding for lesion presence. Sholl analyses were performed >1 week later on deidentified images in an in-house developed interface incorporated in MeVisLab. Markers were placed in the center of A $\beta$ -positive cortical vessels. The cortical ribbon was manually outlined and the resulting area surrounding the masks was divided into 4 concentric shells (each shell measuring 100 pixels in width, which equals 360 $\mu$ m). In each shell, the density of A $\beta$ -positive cortical vessels/mm<sup>2</sup> was calculated. Microbleed size was calculated by measuring the greatest diameter on the H&E section that captured the center of the lesion.

From the same serial sections, all microbleeds and microinfarcts that were annotated on the H&E-stained sections were included for the single-vessel analysis. All stained sections (ie, H&E, A $\beta$ , fibrin[ogen], SMC/A $\beta$ /lectin) surrounding a microbleed or microinfarct were visually inspected to determine whether the presumed "culprit" vessel was visible and to determine presence or absence of A $\beta$ , fibrin(ogen), or SMCs in the wall of the culprit vessel at the lesion site or in the same vessel upstream or downstream from the lesion site. Because immunohistochemistry against A $\beta$  was

performed on section 2, 6, 10, 14, et cetera, individual vessels could be traced to determine the presence or absence of A $\beta$  in detail.

### Statistical Analysis

Correlations for the whole-hemisphere and regional analyses were calculated using Spearman rank correlation coefficients. The CAA severity scores in occipital and parietal cortex (posterior brain areas) and frontal and temporal cortex (anterior brain areas) were averaged and compared with a Wilcoxon signed-rank test for within-case comparisons. Group differences in density of A $\beta$ -positive cortical vessels for the local Sholl analyses were calculated using Mann–Whitney *U* tests. The 2 samples from Cases 2 and 10 were analyzed separately from the sample from Case 4, as they were taken from different anatomical areas of the brain. Differences between diameter of old/chronic and recent/acute microbleeds were calculated with an independent samples *t* test. A chi-squared test was used to determine whether microinfarcts more often had A $\beta$  in the walls of vessels at the site of rupture compared to microbleeds. Graphs were generated in Prism (v5.03; GraphPad Software, San Diego, CA), and statistical analyses were performed in SPSS (v22; IBM, Armonk, NY).

## Results

### Whole-Hemisphere Associations

The brains of 12 autopsy cases (8 males, 4 females; mean age at death = 73 years, range = 64–88) that met the Boston criteria for definite CAA<sup>1</sup> were included in this study (see Table). The median cumulative CAA severity score was 7.5 (range = 5–10 out of a maximum score of 12). On ex vivo 3T MRI, a total number of 1,168 cortical microbleeds (mean =  $97 \pm 88$  per case, range = 4–261) and 472 cortical microinfarcts (mean =  $39 \pm 46$  per case, range = 3–144) were observed (Fig 2). Microbleeds were more often observed in posterior parts of the brain, whereas microinfarcts frequently involved the parts of the brain perfused by end arteries. Neither the number of microbleeds (Spearman  $\rho = 0.426$ ,  $p = 0.17$ ) nor the number of microinfarcts (Spearman  $\rho = -0.278$ ,  $p = 0.38$ ) on ex vivo 3T MRI correlated with cumulative CAA severity score. However, cases with >80 microbleeds on ex vivo 3T MRI ( $n = 6$ ) did have more severe CAA compared to cases with <80 microbleeds ( $n = 6$ ;  $p = 0.050$ ).

### Regional Associations

Given the relatively weak association between microbleeds and microinfarcts and CAA severity at the whole-hemisphere level, we next asked whether microbleeds and microinfarcts were more often observed in regional areas with higher CAA severity. To this end, we assessed microbleeds and microinfarcts histopathologically to correlate directly with CAA severity on the same section. On the H&E-stained sections taken from predefined areas from frontal, temporal, parietal, and occipital cortex, a total number of 13 cortical microbleeds (mean =  $1.1 \pm 1.3$ ,

**TABLE. Case Characteristics and ex vivo MRI and Neuropathological Findings**

Case ID/Sex/Hemisphere	Age at Death, yr/Death Due to Acute ICH	PMI, h	CMBs on ex vivo 3T MRI/CMIs on ex vivo 3T MRI	CAA Severity, Cumulative Score <sup>a</sup>	Other Neuropathological Observations <sup>b</sup>
1/M/R	80/N	Unk	41/115	5	A3B3C2
2/M/L	70/Y	16	261/33	9	A3B3C1, moderate hypertensive vasculopathy
3/M/R	76/N	27	39/21	7	A3B3C2, arteriolosclerosis
4/M/L	65/Y	14	85/144	7	A3B1C2
5/M/R	81/N	Unk	4/12	5	A3B2C2, moderate arteriolosclerosis
6/F/L	70/na	Unk	13/7	6	na
7/M/L	67/N	Unk	109/10	10	A3B3C2
8/M/L	69/Y	36	4/5	10	A3B1C2, mild arteriolosclerosis
9/F/R	64/Y	30	161/3	8	A3B2C3
10/F/R	79/Y	37	204/31	8	A3B3C2
11/M/L	67/N	24	55/27	5	A3B1C1, moderate arteriolosclerosis
12/F/L	88/Y	11	192/64	8	A2B3C2

<sup>a</sup>CAA severity was evaluated on the A $\beta$ -stained sections from the predefined standard areas of frontal, temporal, parietal, and occipital cortex using a 4-point scale (absent, 0; scant A $\beta$  deposition, 1; some circumferential A $\beta$ , 2; widespread circumferential A $\beta$ , 3) following proposed consensus criteria.<sup>13</sup> Scores from the 4 areas were added to form a cumulative CAA severity score.

<sup>b</sup>Extracted from neuropathology reports, based on routine neuropathological examination. ABC score reflects the National Institute on Aging–Alzheimer Association score for Alzheimer disease neuropathologic changes.<sup>36</sup>

CAA = cerebral amyloid angiopathy; CMB = cerebral microbleed; CMI = cerebral microinfarct; F = female; ICH = intracerebral hemorrhage; L = left; M = male; MRI = magnetic resonance imaging; N = no; na = not available; PMI = postmortem interval; R = right; Unk = unknown; Y = yes.

range = 0–4 per case for all areas combined) and 94 cortical microinfarcts (mean =  $7.8 \pm 7.5$ , range = 0–21; Fig 3A) were observed across cases. The number of microbleeds on ex vivo 3T MRI correlated with the total number of microbleeds on histopathology (Spearman  $\rho = 0.572$ ,  $p = 0.052$ ), whereas microinfarcts did not (Spearman  $\rho = 0.452$ ,  $p = 0.14$ ). CAA severity was significantly greater in posterior (occipital and parietal) compared to anterior brain areas (frontal and temporal; see Fig 3B,  $p = 0.005$ ). The number of microbleeds and microinfarcts observed on the H&E-stained sections did not correlate with CAA severity in any area examined (ie, frontal, temporal, parietal, and occipital cortex), except for a negative correlation between CAA severity and the number of microinfarcts in parietal cortex (Spearman  $\rho = -0.630$ ,  $p = 0.028$ ). Also, in line with the whole-hemisphere associations described above, neither the total number of

microbleeds (Spearman  $\rho = 0.124$ ,  $p = 0.701$ ) nor the total number of microinfarcts (Spearman  $\rho = -0.379$ ,  $p = 0.225$ ) on histopathology from all areas combined correlated with cumulative CAA severity score.

In the characterization of the lesions, of the total number of 94 microinfarcts, 61 (65%) were considered old/chronic and 33 (35%) recent/acute (see Fig 3C, D). Two old/chronic microinfarcts showed some evidence of hemorrhagic transformation. With respect to localization, 46 (49%; 31 old, 15 recent) followed the perfusion area of a penetrating cortical arteriole, whereas 48 (51%; 30 old, 18 recent) were located deeper (within layers III–VI) in the cortex. The correlations with regional CAA severity did not notably change when analyzing old/chronic and recent/acute microinfarcts separately.

Of the total number of 13 microbleeds, 12 (92%) were considered old/chronic, and 1 (8%) recent/acute (see

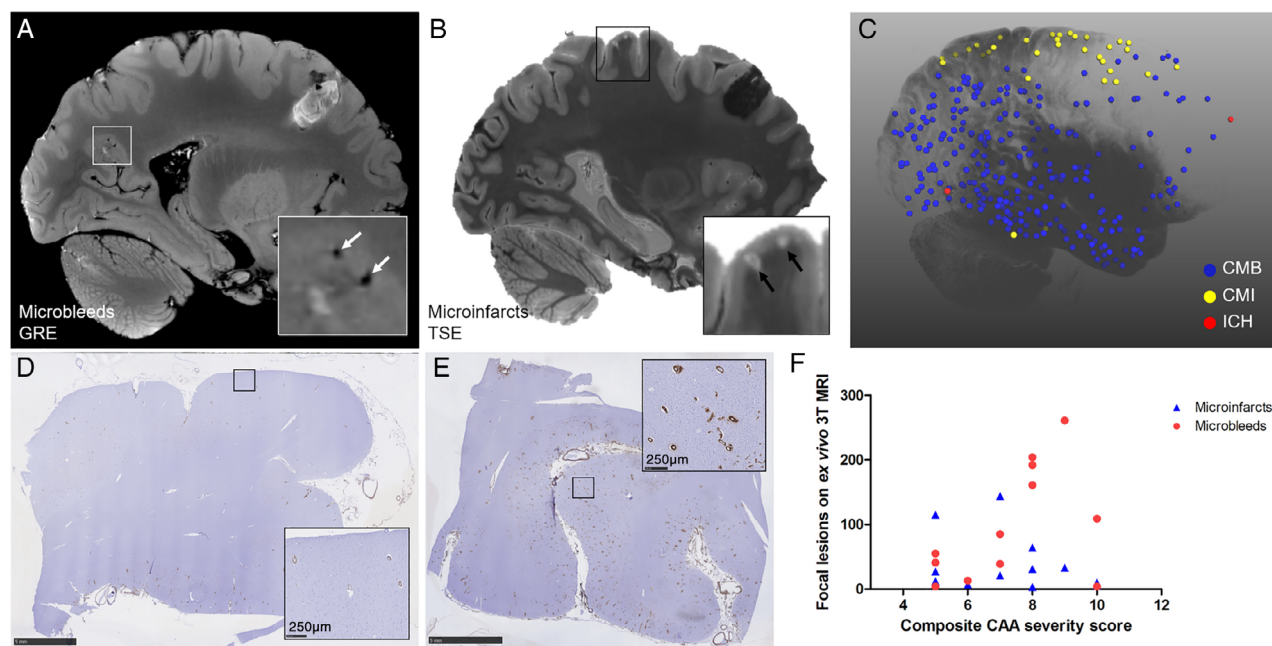


**FIGURE 2:** Whole-brain associations of microbleeds and microinfarcts with cerebral amyloid angiopathy (CAA) severity. (A, B) Cortical microbleeds were assessed on the ex vivo 3T magnetic resonance imaging (MRI) gradient-echo (GRE) scans (A) and cortical microinfarcts on the ex vivo 3T MRI T2-weighted turbo-spin echo (TSE) scans (B). (C) The projection of annotated lesions on a 3-dimensional reconstruction of a representative hemisphere (Case 2) demonstrates that microbleeds (CMB; blue dots) were more often observed in posterior parts of the brain, whereas microinfarcts (CMI; yellow dots) frequently involved the areas of the brain perfused by end arteries. Red dots are areas affected by intracerebral hemorrhage (ICH). (D, E) CAA severity was assessed on standard sections from frontal (D, example of score 1), temporal, parietal, and occipital (E, example of score 3) cortex to create a composite CAA severity score. (F) Neither the number of microbleeds (red circles, Spearman  $\rho = 0.426$ ,  $p = 0.17$ ) nor the number of microinfarcts (blue triangles, Spearman  $\rho = -0.278$ ,  $p = 0.38$ ) were associated with composite CAA severity score. Scale bars in D and E = 5mm.

Fig 3E). In terms of localization, 10 (77%; 9 old, 1 recent) followed the perfusion area of a penetrating cortical arteriole, whereas 3 (23%) were located deeper (within layers III–VI) in the cortex.

### Local Associations

We next asked whether microbleeds or microinfarcts occurred more often in areas with increased CAA severity in the immediate surrounding area. For this analysis, we used the serial sections taken from the temporal cortex in 2 CAA cases (Cases 2 and 10) with many microbleeds in those areas as observed on ex vivo 3T MRI (confirmed with ex vivo 7T MRI). Notably, serial sectioning revealed that microinfarcts were present in these samples as well. As such, a total number of 28 microbleeds (14 old/chronic, 14 recent/acute), 18 microinfarcts (16 old/chronic, 2 recent/acute), and 80 control areas were analyzed (Fig 4A, B). Significantly fewer A $\beta$ -positive cortical vessels were observed in the first shell immediately surrounding a microbleed ( $1.2 \pm 1.8$  vessels/mm<sup>2</sup>) compared to a simulated control lesion ( $2.0 \pm 2.0$  vessels/mm<sup>2</sup>,  $p = 0.023$ ), whereas more A $\beta$ -positive cortical vessels were observed in the first shell immediately surrounding a microinfarct compared to a simulated control lesion ( $3.2 \pm 2.5$  vessels/mm<sup>2</sup>,  $p = 0.054$ ; see Fig 4C, D; each shell is a progressive 360 $\mu$ m area surrounding

a lesion). The difference between microbleeds and simulated control lesions in shell 1 was driven by old/chronic microbleeds ( $p = 0.004$ ) and not recent/acute microbleeds ( $p = 0.57$ ), which became clear after analyzing them separately. Of note, for old/chronic microbleeds, shell 2 also contained significantly fewer A $\beta$ -positive cortical vessels compared to simulated control lesions ( $p = 0.043$ ). This may be the result of the observation that recent/acute microbleeds were significantly larger (greatest diameter on H&E =  $986 \pm 554\mu$ m) compared to old/chronic microbleeds (greatest diameter on H&E =  $397 \pm 268\mu$ m,  $p = 0.002$ ) and therefore the immediate surrounding area of a recent/acute microbleed was likely still occupied with extravasated red blood cells.

To similarly assess local CAA severity surrounding recent/acute microinfarcts (as opposed to old/chronic microinfarcts that were more abundant in the analysis above) we analyzed an independent sample from the parieto-occipital cortex in a third CAA case (Case 4) with many recent/acute microinfarcts in that area as observed on ex vivo 3T MRI (confirmed with ex vivo 7T MRI). A total number of 11 recent/acute microinfarcts and 28 control areas from these serial sections were analyzed independently. Significantly more A $\beta$ -positive cortical vessels were observed in the first shell immediately adjacent to a recent/acute microinfarct

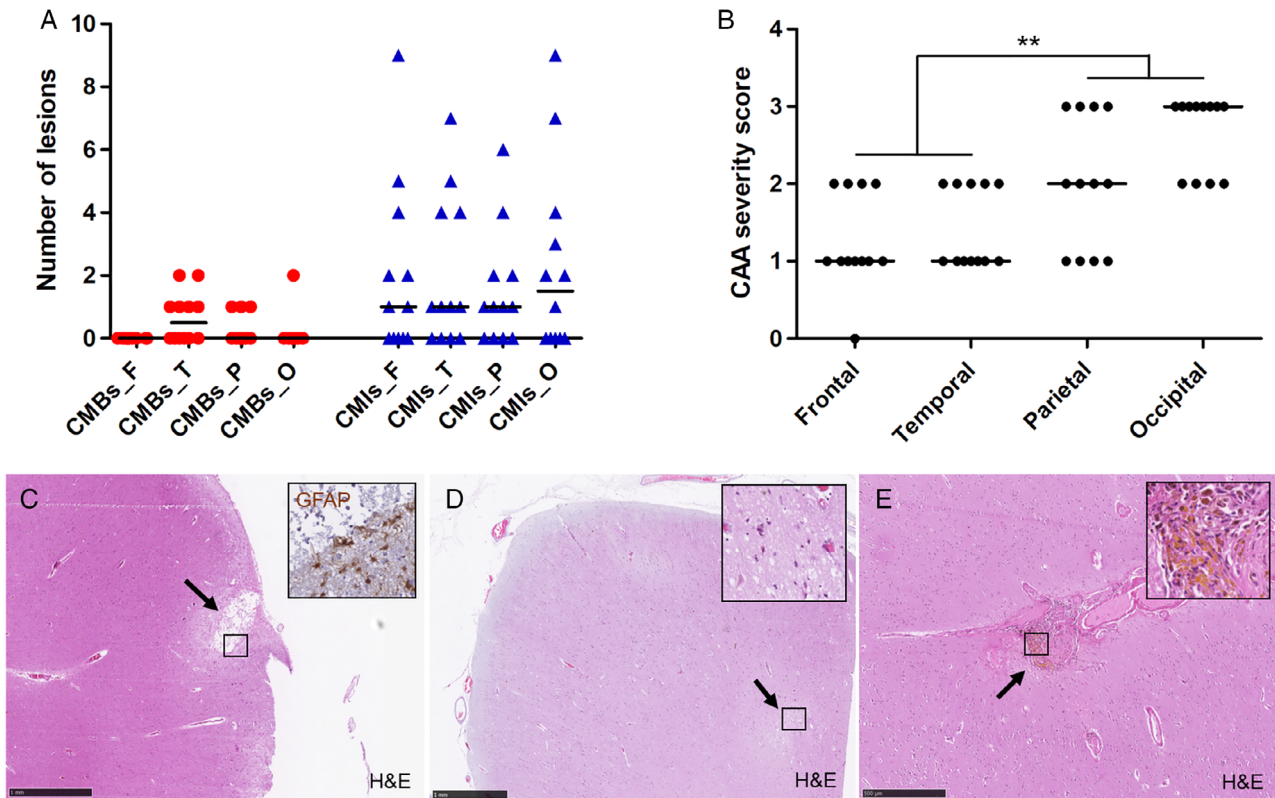


**FIGURE 3:** Regional associations on standard histopathologic examination of microbleeds and microinfarcts with cerebral amyloid angiopathy (CAA) severity. (A, B) On average, CAA severity across all 12 cases followed an anterior-to-posterior distribution (B), whereas number of histopathologically observed cerebral microbleeds (CMBs) and cerebral microinfarcts (CMIIs) did not (A), explaining weak regional associations. (C, D) From the total number of 94 microinfarcts observed on standard histopathology, 61 (65%) were considered old/chronic based on glial fibrillary acidic protein (GFAP) positivity (C, inset; this example follows the perfusion area of a penetrating cortical vessel) and 33 (35%) recent/acute based on the presence of "red: neurons (D, inset; this example is located more deeply, within cortical layer III–VI). (E) From the total number of 13 microbleeds observed on standard histopathology, 12 (92%) were considered old/chronic based on the presence of hemosiderin-containing macrophages (inset), and 1 (8%) was considered recent/acute (not shown). Median is indicated in A and B. Scale bar in C and D = 1mm; scale bar in E = 500 $\mu$ m. F = frontal; H&E = hematoxylin & eosin; O = occipital; P = parietal; T = temporal. \*\* $p < 0.01$ .

( $4.6 \pm 4.8$  vessels/ $\text{mm}^2$ ) compared to a simulated control lesion ( $1.9 \pm 2.0$  vessels/ $\text{mm}^2$ ,  $p = 0.031$ ; Fig 5). These findings suggest that microinfarcts occur in local areas with increased CAA severity.

### Single-Vessel Associations

Finally, we aimed to assess the feeding vessel of each microbleed and microinfarct captured on the serial sections to determine the pathological changes at the level of the individual vessel that presumably caused the lesion. A total number of 28 microbleeds (14 old/chronic, 14 recent/acute) from 2 cases, and 22 microinfarcts (15 old/chronic, 7 recent/acute) from 3 cases were analyzed. The findings from old/chronic and recent/acute lesions were comparable and hence are summarized together. The culprit vessel could be reliably identified in 24 of 28 microbleeds (86%). A $\beta$  was observed in the vessel wall at the rupture site for only 1 (4%) microbleed, whereas A $\beta$  was observed in the vessel wall upstream or downstream for 20 (71%) microbleeds. In 20 of 23 (87%)

available culprit vessels, extensive fibrin(ogen) was present in the wall at the lesion site (the other 3 vessels showed mild fibrin[ogen] deposition). Intact SMCs at the lesion site were observed for only 1 (4%) microbleed (Fig 6A–I). In addition, qualitative analysis after single-vessel tracing over several serial sections revealed that vessels involved in microbleeds were abnormally enlarged arterioles (sometimes showing microaneurysmlike features) and were associated with fibrinoid necrotic changes, and revealed extensive remodeling of the vessel wall extending upstream from the lesion site (Fig 7). Notably, on the same sections, several cortical vessels were observed (on average  $\sim 3$  per H&E section) with the same pathological features (ie, abnormally enlarged arterioles with fibrinoid necrotic changes, loss of SMCs, and loss of A $\beta$  from the wall) but without evidence of hemorrhage (see Fig 7).

From the total number of 22 microinfarcts, in 13 (59%) the presumed culprit vessel(s) could be reliably identified. Vascular A $\beta$  was observed at the core of 20 (91%) microinfarcts ( $p < 0.001$  compared to microbleeds), and for 18 (82%) A $\beta$



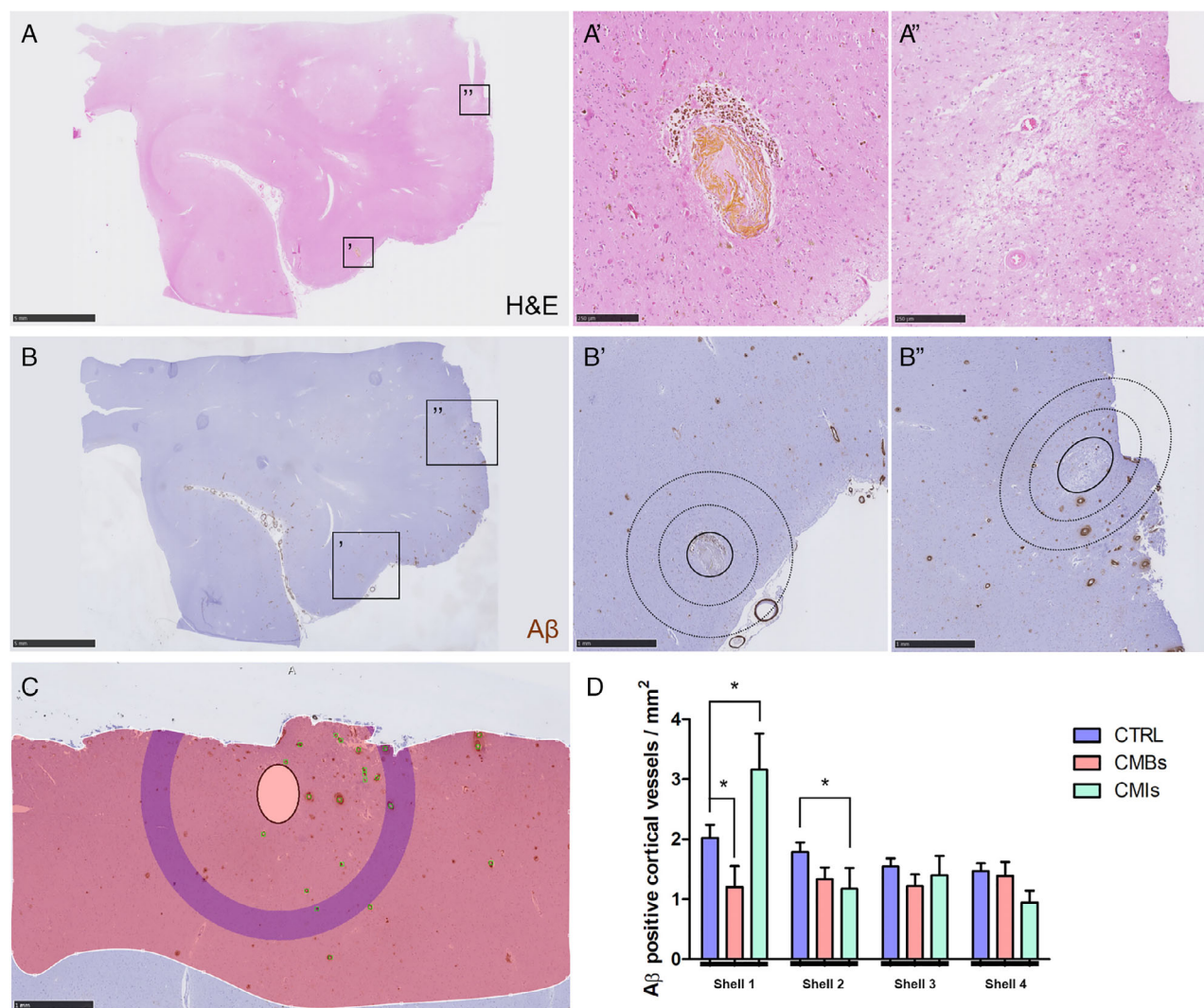


**FIGURE 4:** Local associations of microbleeds and microinfarcts with amyloid  $\beta$  ( $A\beta$ )-positive cortical vessels. (A) Based on the hematoxylin & eosin (H&E)-stained serial sections (A) from the additional samples taken from the temporal cortex in 2 CAA cases, 28 microbleeds ( $A'$ ) and 18 microinfarcts ( $A''$ ) were included. (B) Lesions were localized on the adjacent  $A\beta$ -stained sections to perform Sholl analysis ( $B'$ ,  $B''$ , inner circle with solid outline indicates masked area, circles with dotted outlines indicate first 2 shells). (C) After masking of the lesion,  $A\beta$ -positive cortical vessels were manually annotated (green markers), the cortical ribbon was outlined (red shaded area), and the density of  $A\beta$ -positive cortical vessels was generated by the software for 4 concentric circles extending from the outer border of the masked area (purple concentric circle in this example is shell 4). (D) Significantly fewer  $A\beta$ -positive cortical vessels were observed in the first shell immediately adjacent to a cerebral microbleed (CMB) compared to a simulated control (CTRL) lesion ( $p = 0.023$ ), whereas more  $A\beta$ -positive cortical vessels were observed in the first shell immediately adjacent to a cerebral microinfarct (CMI) compared to a simulated control lesion ( $p = 0.054$ ). For the second shell, significantly fewer  $A\beta$ -positive cortical vessels were observed for microinfarcts compared to simulated control lesions ( $p = 0.039$ ). Scale bars in A and B = 5mm; scale bars in  $B'$ ,  $B''$ , and C = 1mm; scale bars in  $A'$  and  $A''$  = 250 $\mu$ m. Error bars in D = standard error of the mean. \* $p < 0.05$ .

was observed in the vessel wall upstream or downstream from the microinfarct. In 17 (77%) vessels, fibrin(ogen) was present at the core of the microinfarct, but to a relatively mild degree in comparison to microbleeds. Intact SMCs at the lesion site were observed for only 2 (9%) microinfarcts (see Fig 6J–R). In addition, qualitative analysis after single-vessel tracing over several serial sections revealed that vessels involved in microinfarcts appeared as intact arterioles but were presumably "stiff" (ie, heavily  $A\beta$ -occupied walls without SMCs) and with relatively narrow lumens (see Fig 7).

## Discussion

The results from this study revealed several main findings. First, we found that the number of microbleeds detected on ex vivo 3T MRI in cases with CAA correlated with the number of microbleeds observed on standard histopathological sections, whereas the number of microinfarcts did not. This suggests that MRI is sensitive for microbleed detection, but underestimates total microinfarct burden that is present throughout the brain. Microinfarcts appear to greatly outnumber microbleeds in CAA cases. Second,

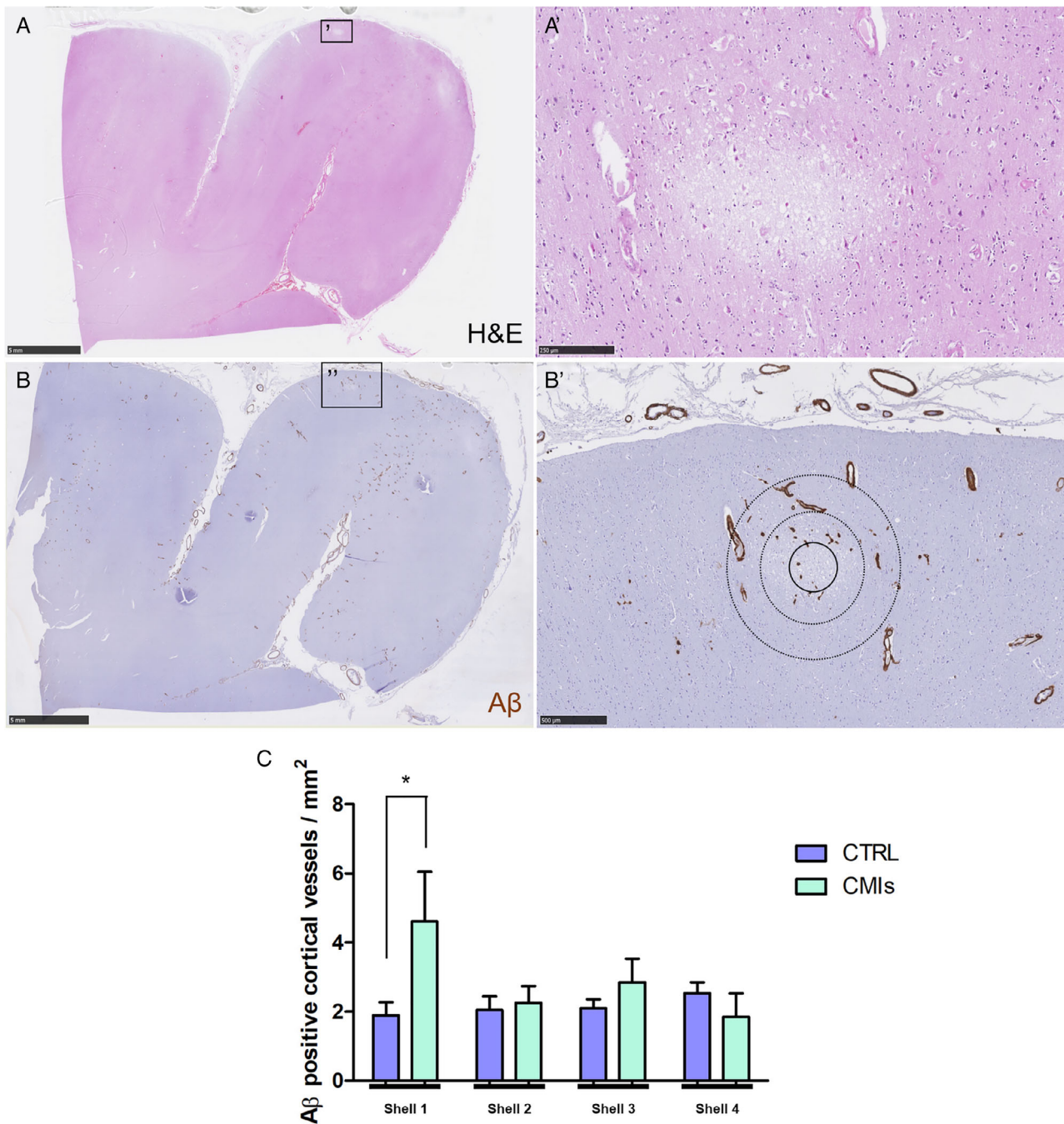


**FIGURE 5:** Local associations of recent/acute microinfarcts with amyloid  $\beta$  ( $A\beta$ )-positive cortical vessels. (A) Based on the hematoxylin & eosin (H&E)-stained serial sections (A) from the third additional sample taken from the parieto-occipital cortex in 1 cerebral amyloid angiopathy case, 11 recent/acute microinfarcts (A') were included. (B) Lesions were localized on the adjacent  $A\beta$ -stained sections (B) to perform Sholl analysis (B', inner circle with solid outline indicates masked area, circles with dotted outlines indicate first 2 shells). (C) Significantly more  $A\beta$ -positive cortical vessels were observed in the first shell immediately adjacent to a cerebral microinfarct (CMI) compared to a simulated control (CTRL) lesion ( $p = 0.031$ ). Scale bars in A and B = 5mm; scale bar in A' = 250 $\mu$ m; scale bar in B' = 500 $\mu$ m. Error bars in C = standard error of the mean. \* $p < 0.05$ .

we found that microbleeds and microinfarcts were not associated with CAA severity at the whole-hemisphere or regional level. Rather, microbleeds and microinfarcts are the results of local changes, as the immediate surrounding local area of a microbleed contained fewer  $A\beta$ -positive cortical vessels compared to simulated control lesions,

whereas microinfarcts happened more often in local areas with an increased number of  $A\beta$ -positive cortical vessels. Third, single-vessel tracing over serial sections revealed that microbleeds are associated with extensive vessel wall remodeling and loss of  $A\beta$  from a single vessel, whereas microinfarcts may be the result of increased  $A\beta$  and

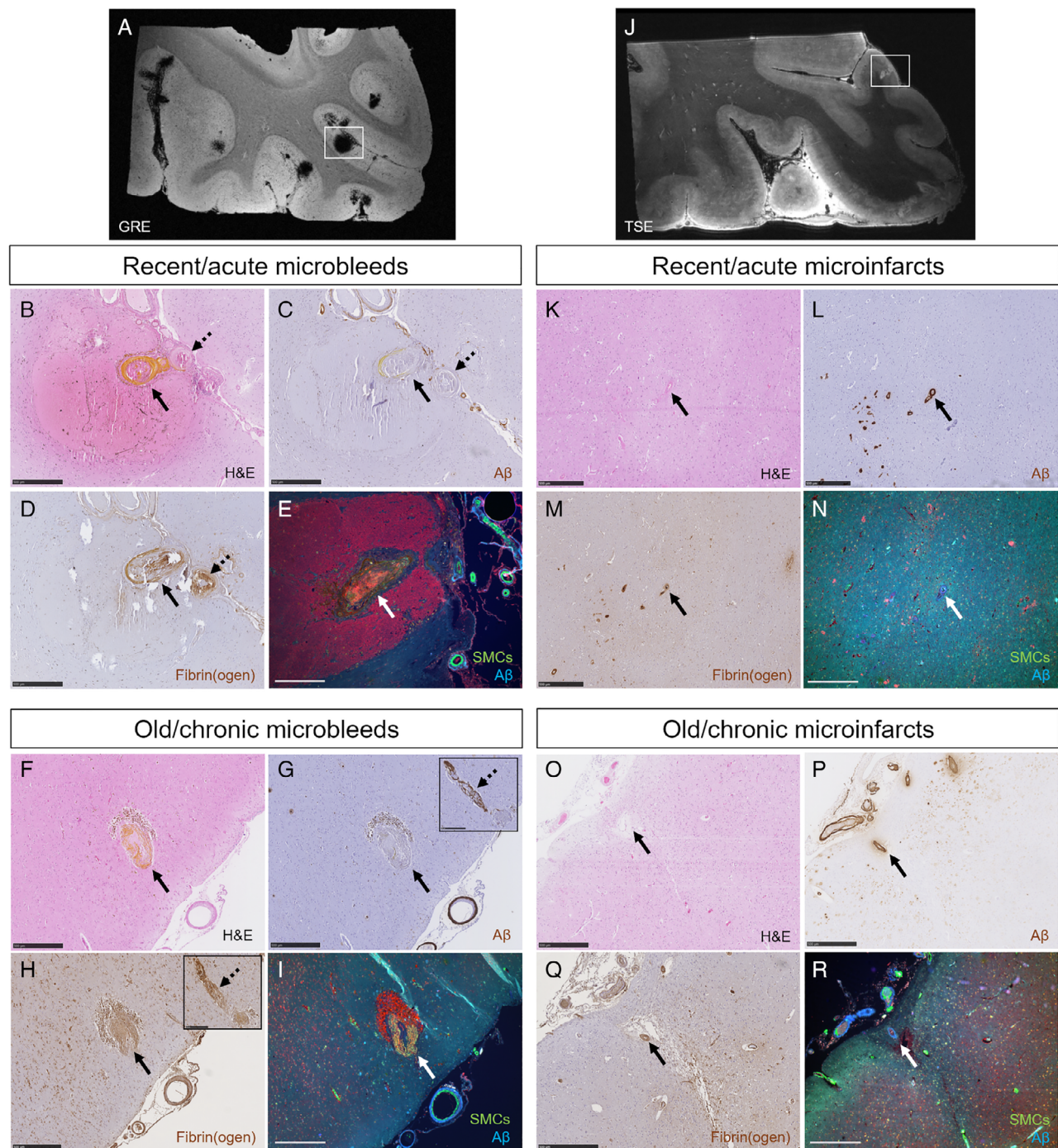


**FIGURE 6:** Single-vessel pathologies of microbleeds and microinfarcts. (A) The high numbers of microbleeds in the additional samples taken from the temporal cortex in 2 cerebral amyloid angiopathy (CAA) cases were confirmed with ex vivo 7T magnetic resonance imaging (MRI). (B, C) Single-vessel analysis on serial sections revealed, for recent/acute microbleeds, absence of amyloid  $\beta$  ( $A\beta$ ) from the vessel wall at the site of bleeding (arrows, yellow substance is hematoidin). In this example, also no  $A\beta$  was observed upstream from the bleeding site (C, broken arrow). (D) Extensive fibrin(ogen) was observed at the rupture site and upstream. (E) No intact smooth muscle cells (SMCs) were observed in the responsible vessel. (F) Similar observations were made for old/chronic microbleeds (brown deposits are hemosiderin-containing macrophages). (G) Note that for this example,  $A\beta$  was not present at the rupture site (arrow), but was observed downstream (broken arrow; inset shows the same vessel captured on a consecutive serial section). (H, I) Extensive fibrin(ogen) was observed both at the rupture site (H; arrow) and downstream (H; broken arrow; inset shows the same vessel captured on a consecutive serial section), but no SMCs (I). (J) The high number of microinfarcts in the additional sample taken from the parieto-occipital cortex in 1 CAA case was confirmed with ex vivo 7T MRI. (K–N) Single-vessel analysis on serial sections revealed, for recent/acute microinfarcts (K), presence of  $A\beta$  in the wall(s) of vessel(s) at the core of the lesion (L), mild fibrin(ogen) deposition (M), and loss of SMCs (N). (O–R) Similar observations were made for old/chronic microinfarcts. All scale bars are 500 $\mu$ m. Note that the lesion in E is a different recent/acute microbleed than in B–D. GRE = gradient-echo; H&E = hematoxylin & eosin; TSE = turbo-spin echo.

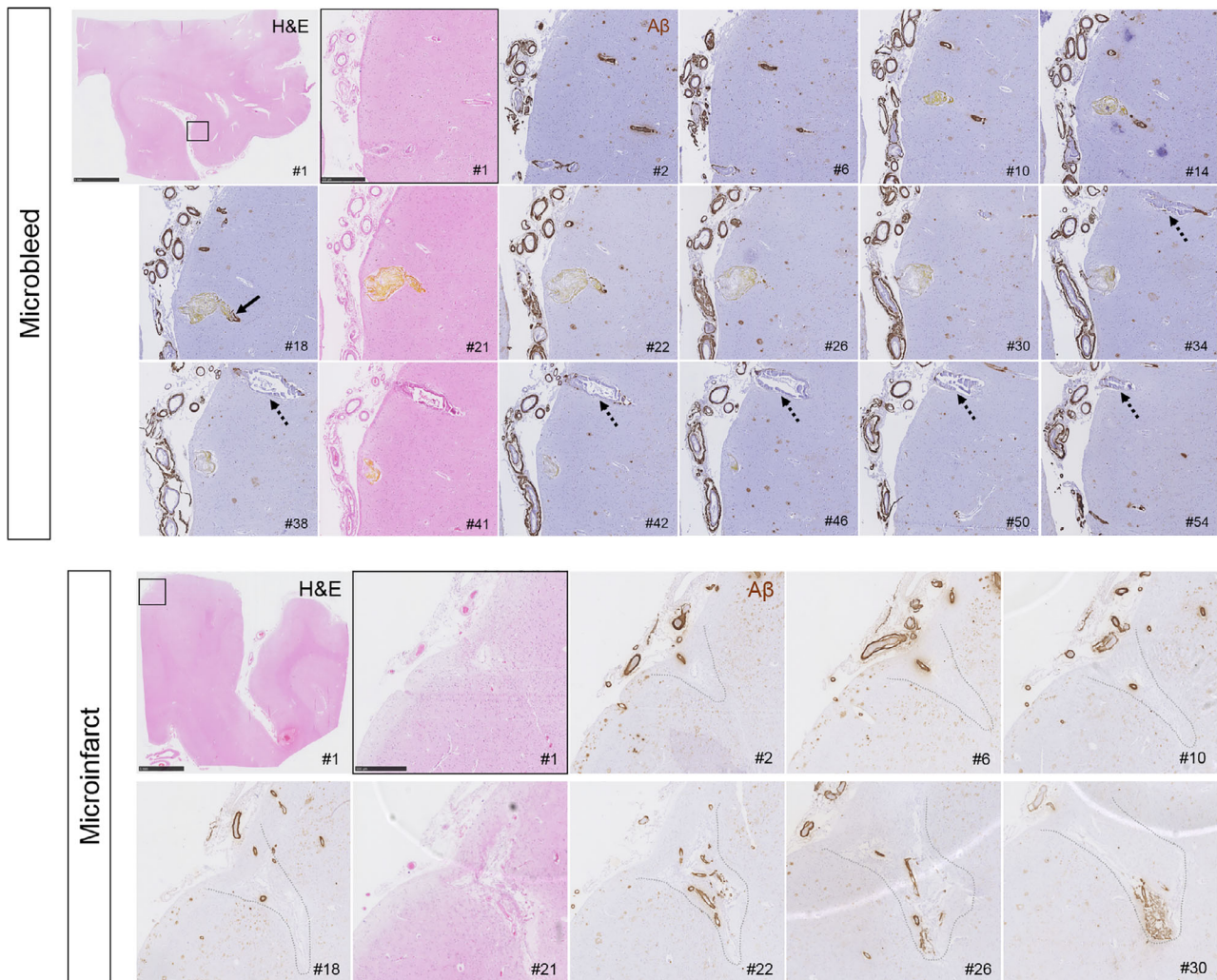


**FIGURE 7:** Serial hematoxylin & eosin (H&E)- and amyloid  $\beta$  (A $\beta$ )-stained sections capturing a recent/acute microbleed and an old/chronic microinfarct. (Top) Vessels responsible for microbleeds were traced on serial sections, stained with H&E (#1, 21, 41, etc) and A $\beta$  (#2, 6, 10, etc), and revealed absence of A $\beta$  at the rupture site, but subtle A $\beta$  upstream and downstream (arrow). This example is a recent/acute microbleed characterized by hematoidin (yellow substance). Note that the vessel is enlarged at the site of bleeding (section #21). Moreover, this vessel did not have any smooth muscle cells (SMCs) left but showed extensive fibrin(ogen) buildup in the wall (not shown). Note the vessel that runs in parallel to the microbleed (broken arrows), which is also abnormally enlarged and shows loss of A $\beta$  from the vessel wall but has not ruptured. Scale bar in first panel = 5mm; scale bar in second panel = 500 $\mu$ m. (Bottom) Microinfarcts were traced on serial sections and stained with H&E (#1, 21, 41, etc) and A $\beta$  (#2, 6, 10, etc), which revealed extensive vascular A $\beta$  at the core of the microinfarcts, as well as upstream and downstream. This example is a chronic/old microinfarct characterized by tissue loss, cavitation, and glial fibrillary acidic protein positivity (not shown). Note that the walls of the vessels at the core of the microinfarct appear relatively intact, except that they lost their SMCs (not shown). Scale bar in first panel = 5mm; scale bar in second panel = 500 $\mu$ m.

presumed vessel stiffening locally. These observations suggest that 2 distinct pathophysiological processes may lead to the formation of either hemorrhagic or ischemic lesions in CAA, and that microbleeds likely happen at a later timepoint in the disease process.

High-resolution ex vivo 3T MRI of intact hemispheres in this study detected approximately 2.5 times more microbleeds compared to microinfarcts across cases. In contrast, standard histopathology revealed 7 times more microinfarcts compared to microbleeds, which is in line with the previously reported high prevalence of microinfarcts as seen on pathology in CAA cases.<sup>14–16</sup> These observations strengthen the notion

that microscopy has superior sensitivity compared to MRI for the detection of microinfarcts, as discussed elsewhere.<sup>5,10,17,18</sup> Whereas the number of microinfarcts detected on MRI did not correlate with the number of microinfarcts detected on histopathology in our study, the number of microbleeds did, confirming the previously reported finding that MRI is sensitive for microbleed detection, capable of capturing even the smallest hemorrhagic lesions.<sup>10</sup> The latter can be attributed to microbleeds benefiting from a blooming effect owing to the high iron content in especially old microbleeds,<sup>12,19</sup> whereas microinfarcts do not. Increasing MRI field strength (eg, to 7T) may prove helpful

to capture a wider spectrum of the total microinfarct burden in the brain.

At the population level, the number of microbleeds on MRI correlated with A $\beta$  burden as detected with positron emission tomography (PET) imaging.<sup>20</sup> Moreover, cortical florbetapir-PET levels were higher in patients with CAA-related acute ICH and lobar microbleeds compared to patients with hypertension-related acute ICH and deep microbleeds.<sup>21</sup> However, the correlation between microbleed numbers and A $\beta$  levels within CAA cases has not been assessed to date, likely due to the relatively small number of patients who have undergone PET imaging.<sup>22</sup> Here, we confirmed the known predilection of microbleeds for posterior brain areas, which corresponded to greater CAA severity in parietal and occipital cortex. However, we did not find a strong relationship between the number of microbleeds and CAA severity at the whole-hemisphere or regional level. The absence of a significant correlation is unlikely to be due to the relatively small sample size, because we recently reported a significant correlation between microbleeds on ex vivo whole-hemisphere 3T MRI and cumulative fibrin(ogen) levels on histopathology.<sup>9</sup> The absence of a correlation between cortical microinfarcts and CAA severity at the whole-brain or regional level may be related to the poor detection of microinfarcts on MRI. Another explanation could be that although cortical microbleeds are rather specific for CAA, cortical microinfarcts have been associated with multiple etiologies, including non-small vessel disease-related conditions such as atrial fibrillation.<sup>5</sup>

At the local level, we reproduced the previously reported observation of fewer A $\beta$ -positive cortical vessels in the immediate surrounding area of a microbleed.<sup>7</sup> This contradicts a widely held belief that bleeding happens as a direct result of increased CAA severity locally. A previous study found an increased A $\beta$  burden in the immediate surrounding areas of microbleeds compared to simulated control lesions using PET imaging in patients with CAA.<sup>23,24</sup> An important difference between the PET study and our histopathology study is the resolution at which A $\beta$  burden was assessed. Owing to the relatively low resolution of PET, shell sizes were set at 2mm each, which is several magnitudes larger compared to the shell size in our study (360 $\mu$ m in diameter). In contrast to microbleeds, we observed more A $\beta$ -positive cortical vessels in the immediate surrounding area of microinfarcts. A possible explanation for this observation could be that the extensive A $\beta$  buildup in vessels surrounding an ischemic area is the result of impaired paravascular clearance of solutes, including A $\beta$ , that occurs after vessel occlusions.<sup>25,26</sup> However, in our study we also found increased numbers of A $\beta$ -positive cortical vessels immediately surrounding recent/acute microinfarcts, which argues against the protein elimination failure hypothesis as an alternative explanation for our findings and suggests that microinfarcts do occur in local areas with higher CAA severity.

Serial sectioning allowed us to make impactful observations at the single-vessel level. First, our findings provide evidence for a scenario in which microbleeds happen in unhealthy enlarged CAA-affected vessels due to A $\beta$ -induced degeneration of SMCs, fibrin(ogen) buildup, extensive vessel wall remodeling, and loss of A $\beta$  locally. The presence of several vessels on the microbleed-containing sections that had undergone very similar pathologic changes but had not ruptured provides further evidence for this scenario. Our findings also fit well with early observations of fibrinoid necrotic vessels and microaneurysms in brains with CAA-related hemorrhages<sup>27</sup> and more recently reported associations between microbleeds and fibrin(ogen) in patients with CAA.<sup>9</sup> Collectively, these data suggest that extensive buildup of A $\beta$  in the walls of arterioles alone is not enough for the vessel to become fragile and rupture, but that it must undergo remodeling as well. This is in line with recent transcriptomic studies in patients with hereditary CAA (Dutch-type) that found upregulation of extracellular matrix-related pathways and transforming growth factor  $\beta$ -induced profibrotic genes.<sup>28,29</sup> Second, our findings provide evidence that microinfarcts happen in intact CAA-affected arterioles that are characterized by extensive A $\beta$  buildup, loss of SMCs, and luminal narrowing. These vessels likely predispose to hypoperfusion and/or occlusions. We did not observe individual small thrombi or emboli in penetrating cortical arterioles that would have provided direct evidence for occlusion. However, our methods may not have been sensitive enough to detect (often temporary) small-caliber vessel occlusions in 2D postmortem tissue sections. The typical topographical distribution of microinfarcts in cortical areas that are perfused by end arteries points to hypoperfusion as another likely contributing mechanism for ischemia surrounding CAA-affected vessels.<sup>30–33</sup> Reduced vascular reactivity due to vessel stiffness in areas at risk of microinfarction may be an interesting early biomarker.<sup>34</sup> It is also possible that the single-vessel observations for microbleeds and microinfarcts reflect shared pathophysiological mechanisms that are captured at different timepoints in the evolution of the disease. This is supported by the observation that microinfarcts precede microbleeds on in vivo MRI in patients with Dutch-type CAA.<sup>35</sup> It may also explain the higher number of microinfarcts present in our CAA cases, which may have accumulated over a longer time period. A major unanswered question is why one affected vessel undergoes remodeling and another results in a microinfarct. Complex flow dynamics that differently affect separate locations within the larger connected vascular network likely play a role. Future experimental studies are needed to address this question in greater detail.

An important limitation of postmortem studies is their cross-sectional nature, which makes it challenging to infer causes and consequences based on single neuropathological observations. An important alternative explanation

for our observations is that bleeding from a vessel may result in loss of A $\beta$  and vessel wall thickening, either directly or indirectly through local inflammatory responses. However, 2 important observations argue against this alternative explanation: (1) the absence of A $\beta$  from walls that had recently (<24 hours) ruptured (see Fig 6B, C), because macrophages that take up red blood cells (and possibly A $\beta$ ) infiltrate the tissue >24 hours after a bleeding event; and (2) the presence of similarly abnormally enlarged vessels with fibrin(ogen) in the wall and reduced A $\beta$ , but no evidence of bleeding (see Fig 7). Because hemosiderin-containing macrophages remain present in the tissue for months up to years, it is most likely that these abnormal vessels without hemosiderin in the surrounding tissue represent vessels that had not bled. The observation of fibrin within astrocytes next to these vessels suggests that the blood–brain barrier was already compromised, rendering these abnormal vessels at risk for subsequent bleeding. Another limitation related to the nature of this autopsy study is the relatively small number of cases that were included. Given the case-to-case variability, reflected in the wide range of detected lesions, it cannot be excluded that some cases contributed more than others to the observed associations. External validation in larger datasets therefore is preferred.

Our findings provide support for the notion that a single neuropathologic process, such as CAA, can produce 2 different types of lesions (ie, hemorrhages and ischemic tissue injury), possibly by 2 distinct pathophysiological mechanisms. This framework has implications for other forms of cerebral small vessel diseases (such as hypertensive arteriopathy), for which CAA can provide a model to understand lesion formation. Our findings also have implications for anti-A $\beta$  antibody trials suggesting that the removal of A $\beta$  at a late disease stage from vessels that have already lost their SMCs and have undergone extensive remodeling may increase the risk of bleeding. The focus should therefore be on early treatment to prevent extensive A $\beta$  buildup in the walls of small vessels, thereby lowering the risk of lesion formation in patients with CAA or Alzheimer disease.

## Acknowledgment

The work described in this study was supported by the NIH (NINDS R01 NS096730, NIA K99 AG059893, NINDS RF1 NS110054, and NIA R21 AG046657) and the Netherlands Organization for Scientific Research (Rubicon fellowship 019.153LW.014 and Veni 91619021).

We thank the families of the patients who generously donated their brains to our research studies, and

N. Clement for his excellent assistance in the autopsy procedures.

## Author Contributions

S.J.v.V., B.J.B., M.P.F., and S.M.G. contributed to the conception and design of the study; S.J.v.V., A.A.S., W.M.F., A.t.T., A.J.v.d.K., and M.P.F. contributed to the acquisition and analysis of the data; S.J.v.V. drafted the text and prepared the figures.

## Potential Conflicts of Interest

Nothing to report.

## References

- Greenberg SM, Charidimou A. Diagnosis of cerebral amyloid angiopathy: evolution of the Boston criteria. *Stroke* 2018;49:491–497.
- Greenberg SM, Vernooij MW, Cordonnier C, et al. Cerebral microbleeds: a guide to detection and interpretation. *Lancet Neurol* 2009;8:165–174.
- Reijmer YD, Fotiadis P, Martinez-Ramirez S, et al. Structural network alterations and neurological dysfunction in cerebral amyloid angiopathy. *Brain* 2015;138:179–188.
- Reijmer YD, Van Veluw SJ, Greenberg SM. Ischemic brain injury in cerebral amyloid angiopathy. *J Cereb Blood Flow Metab* 2016;36:40–54.
- Van Veluw SJ, Shih AY, Smith EE, et al. Detection, risk factors, and functional consequences of cerebral microinfarcts. *Lancet Neurol* 2017;16:730–740.
- Charidimou A, Boulouis G, Gurol ME, et al. Emerging concepts in sporadic cerebral amyloid angiopathy. *Brain* 2017;140:1829–1850.
- Van Veluw SJ, Kuijff HJ, Charidimou A, et al. Reduced vascular amyloid burden at microhemorrhage sites in cerebral amyloid angiopathy. *Acta Neuropathol* 2017;133:409–415.
- Van Veluw SJ, Reijmer YD, Van der Kouwe AJ, et al. Histopathology of diffusion imaging abnormalities in cerebral amyloid angiopathy. *Neurology* 2019;92:e933–e943.
- Freeze WM, Bacskai BJ, Frosch MP, et al. Blood-brain barrier leakage and microvascular lesions in cerebral amyloid angiopathy. *Stroke* 2019;50:328–335.
- Van Veluw SJ, Charidimou A, Van der Kouwe AJ, et al. Microbleed and microinfarct detection in amyloid angiopathy: a high-resolution MRI-histopathology study. *Brain* 2016;139:3151–3162.
- Dale AM, Fischl B, Sereno MI. Cortical surface-based analysis. I. Segmentation and surface reconstruction. *Neuroimage* 1999;9:179–194.
- Van Veluw SJ, Biessels GJ, Klijn CJ, Rozemuller AJ. Heterogeneous histopathology of cortical microbleeds in cerebral amyloid angiopathy. *Neurology* 2016;86:867–871.
- Love S, Chalmers K, Ince P, et al. Development, appraisal, validation and implementation of a consensus protocol for the assessment of cerebral amyloid angiopathy in post-mortem brain tissue. *Am J Neurodegener Dis* 2014;3:19–32.
- Soontornniyomkij V, Lynch MD, Mermash S, et al. Cerebral microinfarcts associated with severe cerebral beta-amyloid angiopathy. *Brain Pathol* 2010;20:459–467.
- Kövari E, Herrmann FR, Hof PR, Bouras C. The relationship between cerebral amyloid angiopathy and cortical microinfarcts in brain

- ageing and Alzheimer's disease. *Neuropathol Appl Neurobiol* 2013; 39:498–509.
16. Ringman JM, Sachs MC, Zhou Y, et al. Clinical predictors of severe cerebral amyloid angiopathy and influence of APOE genotype in persons with pathologically verified Alzheimer disease. *JAMA Neurol* 2014;71:878–883.
  17. Westover MB, Bianchi MT, Yang C, et al. Estimating cerebral microinfarct burden from autopsy samples. *Neurology* 2013;80: 1365–1369.
  18. Van Veluw SJ, Zwanenburg JJ, Engelen-Lee J, et al. In vivo detection of cerebral cortical microinfarcts with high-resolution 7T MRI. *J Cereb Blood Flow Metab* 2013;33:322–329.
  19. Schrag M, McAuley G, Pomakian J, et al. Correlation of hypointensities in susceptibility-weighted images to tissue histology in dementia patients with cerebral amyloid angiopathy: a postmortem MRI study. *Acta Neuropathol* 2010;119:291–302.
  20. Graff-Radford J, Botha H, Rabinstein AA, et al. Cerebral microbleeds: prevalence and relationship to amyloid burden. *Neurology* 2019;92: e253–e262.
  21. Raposo N, Planton M, Péran P, et al. Florbetapir imaging in cerebral amyloid angiopathy-related hemorrhages. *Neurology* 2017;89: 697–704.
  22. Charidimou A, Farid K, Baron JC. Amyloid-PET in sporadic cerebral amyloid angiopathy: a diagnostic accuracy meta-analysis. *Neurology* 2017;89:1490–1498.
  23. Dierksen GA, Skehan ME, Khan MA, et al. Spatial relation between microbleeds and amyloid deposits in amyloid angiopathy. *Ann Neurol* 2010;68:545–548.
  24. Gurol ME, Dierksen G, Betensky R, et al. Predicting sites of new hemorrhage with amyloid imaging in cerebral amyloid angiopathy. *Neurology* 2012;79:320–326.
  25. Garcia-Alloza M, Gregory J, Kuchibhotla KV, et al. Cerebrovascular lesions induce transient  $\beta$ -amyloid deposition. *Brain* 2011;134: 3697–3707.
  26. Arbel-Ornath M, Hudry E, Eikermann-Haerter K, et al. Interstitial fluid drainage is impaired in ischemic stroke and Alzheimer's disease mouse models. *Acta Neuropathol* 2013;126:353–364.
  27. Vonsattel JP, Myers RH, Hedley-Whyte ET. Cerebral amyloid angiopathy without and with cerebral hemorrhages: a comparative histological study. *Ann Neurol* 1991;30:637–649.
  28. Grand-Moursel L, Munting LP, Van der Graaf LM, et al. TGF $\beta$  pathway deregulation and abnormal phospho-SMAD2/3 staining in hereditary cerebral hemorrhage with amyloidosis-Dutch type. *Brain Pathol* 2018;28:495–506.
  29. Grand-Moursel L, Van Roon-Mom WMC, Kielbasa SM, et al. Brain transcriptomic analysis of hereditary cerebral hemorrhage with amyloidosis-Dutch type. *Front Aging Neurosci* 2018;10:102.
  30. Suter OC, Sunthorn T, Kraftsik R, et al. Cerebral hypoperfusion generates cortical watershed microinfarcts in Alzheimer disease. *Stroke* 2002;33:1986–1992.
  31. Okamoto Y, Yamamoto T, Kalaria RN, et al. Cerebral hypoperfusion accelerates cerebral amyloid angiopathy and promotes cortical microinfarcts. *Acta Neuropathol* 2012;123:381–394.
  32. Van Veluw SJ, Hilal S, Kuijf HJ, et al. Cortical microinfarcts on 3T MRI: clinical correlates in memory-clinic patients. *Alzheimers Dement* 2015;11:1500–1509.
  33. Kapasi A, Leurgans SE, James BD, et al. Watershed microinfarct pathology and cognition in older persons. *Neurobiol Aging* 2018;70: 10–17.
  34. Dumas A, Dierksen GA, Gurol ME, et al. Functional magnetic resonance imaging detection of vascular reactivity in cerebral amyloid angiopathy. *Ann Neurol* 2012;72:76–81.
  35. Van Rooden S, Van Opstal AM, Labadie G, et al. Early magnetic resonance imaging and cognitive markers of hereditary cerebral amyloid angiopathy. *Stroke* 2016;47:3041–3044.
  36. Hyman BT, Phelps CH, Beach TG, et al. National Institute on Aging-Alzheimer's Association guidelines for the neuropathologic assessment of Alzheimer's disease. *Alzheimers Dement* 2012;8:1–13.